Macromolecules
ARTICLE

Macromolecules **2010**, *43*, 8651–8655 **8651**
DOI: 10.1021/ma101827u

Monitoring PMMA Elimination by Reactive Ion Etching from a Lamellar PS-*b*-PMMA Thin Film by *ex Situ* TEM Methods

Richard A. Farrell,[†,‡,§] Nikolay Petkov,[§,∥] Matthew T. Shaw,[‡,⊥] Vladimir Djara,[§] Justin D. Holmes,[†,‡,§] and Michael A. Morris*[,†,‡,§]

[†]*Materials and Supercritical Fluid Group, Department of Chemistry, University College Cork, Cork, Ireland,* [‡]*Centre for Research on Adaptive Nanostructures and Nanodevices (CRANN), Trinity College Dublin, Dublin 2, Ireland,* [§]*Micro-Nano Electronics Centre, Tyndall National Institute, Lee Matings, Prospect Row, Cork, Ireland,* [∥]*Electron Microscopy and Analysis Facility (EMAF), Tyndall National Institute, Lee Maltings, Prospect Row, Cork, Ireland, and* [⊥]*Intel Ireland limited, Collinstown Industrial Estate, Leixlip, Co. Kildare, Ireland*

Received August 10, 2010; Revised Manuscript Received August 27, 2010

ABSTRACT: Block copolymer thin films require selective elimination of one of their constituent blocks to access their potential as lithographic nanopatterns. This paper demonstrates an on-substrate TEM-based approach for establishing the removal of poly(methyl methyacrylate) from vertically oriented lamellar polystyrene-*block*-poly(methyl methacrylate) (PS-*b*-PMMA) thin films and subsequent transfer to the underlying silicon by reactive ion etching. The *ex situ* microscopy technique presents an insight into the removal of PMMA, the etch end point, PS faceting, etch anisotropy, and residual PS thickness.

Recent advances in directed self-assembly (DSA) of block copolymers (BCP) into device-oriented geometries have prompted researchers to investigate and explore methods for transferring and simultaneously characterizing these aligned nanopattern systems.[1−4] To date, numerous research groups have shown the importance of pattern transfer and have made significant strides in advancing these techniques using them to create both memory and logic devices.[4−16]

In general, block copolymer films require either wet (chemical) or dry (plasma) etching techniques to fulfill their templating and pattern transfer potential.[5−11] For example, a common method for PMMA elimination from polystyrene-*block*-poly poly(methyl methacrylate) films is to expose the films to a DUV (< 250 nm) source followed by a development step with acetic acid,[10] whereas Zhang et al. have developed a wet chemical etch technique by introducing a cleavable trityl ether juncture between the PS and PEO bond of a polystyrene-*block*-polyethylene (PS-*b*-PEO) film, which is easily removed in an appropriate acid without any damage to the surrounding polystyrene matrix.[5,8] More recently, reactive ion etching (RIE) has emerged as the preferred technique for removing the oxygen-rich domain from the block copolymer nanopattern as the process is not affected by the capillary actions of solvents.[6] Moreover, RIE processes can be tuned to provide etch selectivity between different polymer blocks (oxygen-containing versus aromatic) and is preferred for high volume manufacturing and throughput.

The fidelity of the pattern transfer is critical since the block polymer films in question are routinely 30−60 nm thick. Etch characteristics such as etch rate, individual polymer block selectivity, sidewall profile, and surface roughness become more stringent as the critical dimension (CD) reduces.[12,13] Liu et al. compared wet and dry processes for etching symmetric PS-*b*-PMMA thin films.[6] The authors noted that wet etching (UV exposure at 250 nm, ∼1 W followed by acetic acid development step) can lead to pattern shifting and is, therefore, not appropriate at these nanoscale dimensions.[6] They also investigated the effect of argon and oxygen plasma chemistries on the etch rate, critical dimension control, and PMMA elimination. The argon etch process showed high etch rate and poor selectivity, while the oxygen plasma conditions resulted in only minor faceting of the PS profile. Their process required a slight overetching of the PMMA component which resulted in 50% of the original PS thickness being consumed (final thickness ∼20 nm). The authors noted that such a loss in PS thickness was not ideal as it limited pattern transfer to low aspect ratio structures. To enhance etch contrast within block copolymer films, polystyrene-*block*-polyferrocenyldimethylsilane,[14,15] polystyrene-*block*-polydimethylsiloxane,[16] and silsesquioxane/PS−PEO hybrid systems[17] are ideal as one of the constituent blocks contains a heavy element which is important for etch resistance.

Techniques for accessing etch characteristics at such small dimensions are vital. The workhorse instrument for block copolymer studies—the atomic force microscope (AFM)—is ineffective for pattern transfer analysis as it cannot provide information on the etch end point while scanning electron microscopy (SEM) is limited due to charging effects, requires metallic coatings, is prone to beam damage and carbon deposition during imaging at ultrahigh resolution, and, last but not least, has limited resolution. To gain insight into the polydomain structure on thin film samples, researchers have used transmission electron microscopy (TEM) and stained one of the blocks (usually the block with a double bond) with strong oxidizers of ruthenium and osmium to create contrast variation.[18,19] TEM provides nanometer scale analysis of the polydomain structure without charging effects and can ultimately determine the true morphology of block copolymer thin films.[20] Researchers have availed of this technique to observe BCP patterns when transferred to silicon,[9,21] but to date no imaging of the selective block removal step or residual polymer profile has been reported in the literature. Furthermore, TEM requires time-consuming sample preparation (microtoning) and sample staining whereas the SEM and AFM techniques do not. In

*To whom correspondence should be addressed: Tel +353 214 902 180; Fax +353 214 274 097; e-mail m.morris@ucc.ie.

Published on Web 10/04/2010

Table 1. As-Deposited and Postetch Homopolymer Film Thickness, Etch Rates, Gas Flow Rates, and PS to PMMA Selectivity for 2 wt % PS and 4 wt % PMMA Homopolymer Films after 1 min of Etching[a]

process no.	RIE power (W)	O_2 flow rate (sccm)	CHF_3 flow rate (sccm)	PMMA etch rate (nm/min)	PS etch rate (nm/min)	PS to PMMA etch selectivity
1	50	50	0	300	146	2.1
2	60	50	0	152	108	1.4
3	70	70	0	130	104	1.3
4	150	5	40	44.0	18.0	2.4
5	150	25	20	182.7	74.7	2.4
6	100	10	40	54.0	26.0	2.1
7	100	5	40	45.0	13.0	3.5
8	100	2	40	13.0	5.0	2.6
9	60	5	40	21.0	13.0	1.6

[a] Etch 7 was used for all diblock copolymer etching. Base pressure and temperature were set at 10 mTorr and 10 °C, respectively.

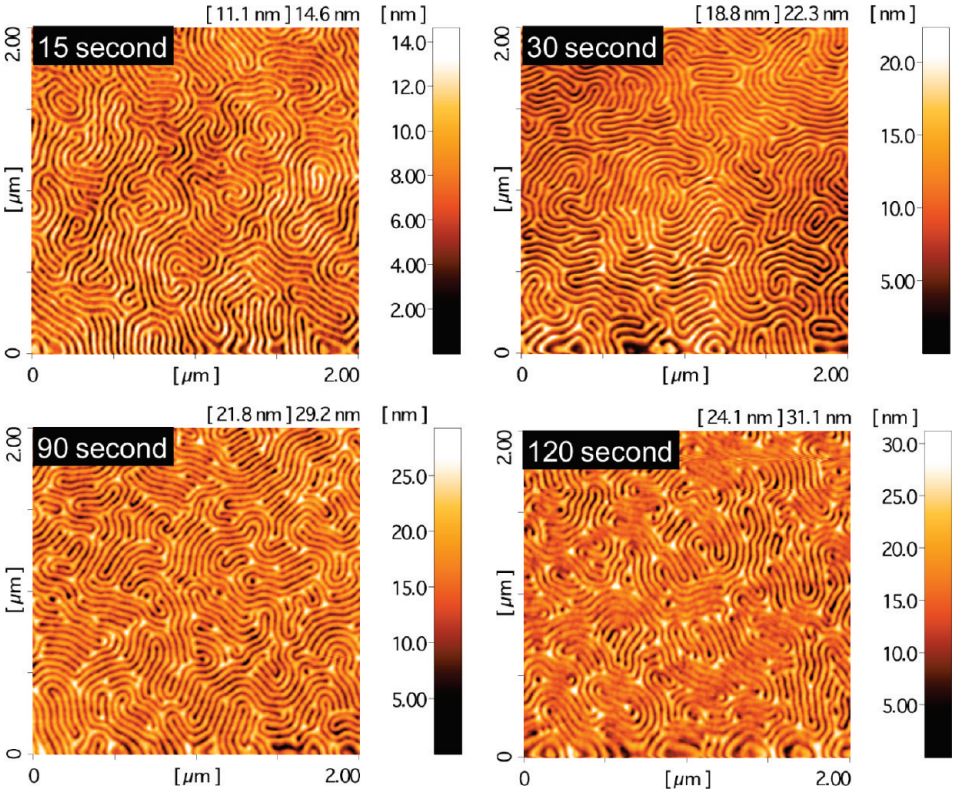

Figure 1. AFM topographic 2 × 2 μm scans for 15, 30, 90, and 120 s etch intervals of a 1.5 wt % PS-*b*-PMMA film deposited on a neutral PS-*r*-PMMA brush layer and annealed for 120 h under vacuum at 180 °C.

summary, no stand-alone microscopy technique can provide all the information required to understand and characterize block copolymer films.

Herein we present a combined approach to solve some of aforementioned pattern transfer issues and show that *ex situ* TEM cross-sectional analysis in conjunction with metal contrast layers can provide important information during the polymer removal step. Properties such as precision etch rate/etch rate variation, anisotropic behavior, and presence of residual layer/incomplete etch ultimately influence the overall pattern transfer. In the following paper, a symmetric PS-*b*-PMMA film with a vertical orientation was chosen as it has an ideal structure for pattern transfer. Progressive PMMA removal and transfer to the underlying silicon was monitored by TEM cross-sectional analysis. The imaging of PMMA removal is made possible by depositing thin Au layers by room temperature electron beam evaporation to provide contrast during image and to act as protective layer during the TEM preparation. A mixture of trifluoromethane (CHF_3) and oxygen (O_2) was chosen for the PMMA etch removal step while a silicon pentaflouride (SF_6) and octafluorocyclobutane (C_4F_8) mixture was employed for transferring the pattern to the underlying bulk silicon substrate.

Experimental Section

Thin Film Deposition. A symmetric polystyrene-*block*-poly poly(methyl methacrylate) (PS-*b*-PMMA) copolymer with a molecular weight of 74 kg mol^{-1} and a neutral polystyrene-*random*-poly(methyl methacrylate) (PS-*r*-PMMA) with a PS content of 58% were purchased from Polymer Source of Canada. For this study, a 1.5 wt % solution of PS-*b*-PMMA in toluene was deposited at 3000 rpm on PS-*r*-PMMA brush layer. The brush layer was deposited by spin-coating and annealed for 72 h at 180 °C. A thin 4−6 nm layer remains after repeated washing of the nonreacted PS-*r*-PMMA layer in toluene. For homopolymer films, solution concentrations of 2 wt % polystyrene (PS) and 4 wt % poly(methyl methacrylate) (PMMA) were used. This provided homopolymer films with final thickness values in the range of 100 to 150 nm which were used to establish preliminary etch rates. Block copolymer films were annealed at 180 °C under vacuum for 120 h.

Reactive Ion Etching. PMMA dry etch removal was performed with an Oxford plasmatech 100 system in RIE mode using various O_2 and CHF_3 mixtures at a pressure of 10 mTorr at 10 °C. For homopolymer etching both PS and PMMA films were loaded within the same etch sequence to ensure both films were exposed to identical processing. Transfer of the pattern to the silicon substrate (STS AOE) was performed on STS AOE system using an SF_6 and C_4F_8 mixture in ICP mode at a pressure of 15 mTorr at 10 °C. The C_4F_8 flow rate was 90 sccm, and the SF_6 flow rates were varied from 20 to 40 sccm.

Thin Film/Nanostructure Characterization. A J.A. Woolam (M-2000U) spectroscopic ellipsometer was used to measure homopolymer film thicknesses before and after RIE. Scanning probe microscopy measurements were performed using a DME DS-50 dual scope in tapping mode. SEM images were obtained using Hitachi S4800 cold emission microscope and FEI Dual-Beam Strata 400 operating between 2 and 10 kV. In order to minimize charging effects, samples were coated with a thin layer of Au/Pd. TEM samples first received a 25 nm gold protective layer by electron beam evaporation (Temescal FC-2000) at room temperature, and cross-sectional samples were prepared using a sequence of grinding and precision Ar-ion polishing (PIPS) steps (Gatan model 691, PIPS operating at 5 kV and incidence angles between 2° and 5°), resulting in a region of electron transparency at the thin film/silicon interface (see Supporting Information S1). Cross-sectional images of the etched films were taken on a JEOL 2000 FX operating at 200 kV.

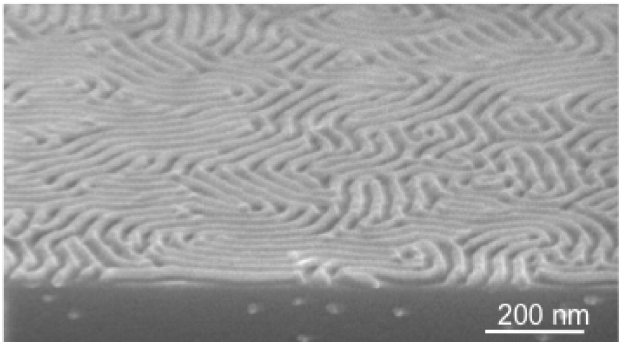

Figure 2. 70° tilt SEM image of a 1.5 wt % PS-*b*-PMMA film post 120 s RIE with flow rates of 40 sccm CHF_3/5 sccm O_2 at 10 mTorr.

Results and Discussion

To estimate the etch rate of the individual PS and PMMA blocks and more importantly to establish the ideal conditions for achieving selectivity of PS over PMMA, etch rates of homopolymer films were investigated in a similar approach to methods outlined elsewhere.[5−7] A significant body of research concerning the RIE of PS-*b*-PMMA with oxygen has been published to date, where etch selectivities of ~ 2.0 have been achieved. Asakawa developed an empirical model based on etching a range of homopolymer films and concluded that the higher the oxygen content within the polymer backbone, the faster the etch rate was for a specified set of parameters using CF_4 RIE.[5] As PMMA contains an ether linkage, and PS is an aromatic hydrocarbon, selectivity between the two polymers is possible. Table 1 lists the gas flow rates for CHF_3 and oxygen O_2 mixtures, homopolymer film thickness, resultant etch rates, and PS to PMMA selectivity for a series of RIE cycles in an Oxford Plasmalab 100 system. Homopolymer film thickness was measured by ellipsometry using a Cauchy fitting model. The initial PS and PMMA film thicknesses were approximately 120 and 130 nm, prior to etching. Pure O_2-etch processes were initially investigated and were found to be inappropriate due to high etch rate and low selectivity (processes 1−3, Table 1). Consequently, the CHF_3/O_2 chemistry was introduced in an attempt to reduce etch rate and increase selectivity owing to the polymerization properties of CHF_3.[22] It was found that a mixture of CHF_3/O_2 with the following flow rates of 40 sccm/5 sccm provided a PMMA etch rate of 45 nm/min but more importantly a reduced etch rate for PS of 13 nm/min over the same time window (Table 1, process 7). This represented an etch selectivity of PS to PMMA of 3.5 for the PS and PMMA homopolymer films.

Based on the conditions identified for homopolymer etching, PS-*b*-PMMA films were exposed to identical plasma conditions (process 7, 40 sccm CHF_3/5 sccm O_2) for different etch times ranging from 15 to 120 s and examined *ex situ* at various intervals. Both AFM and SEM in top-down configuration can be used to detect PMMA etching but cannot detect the end point of the etch

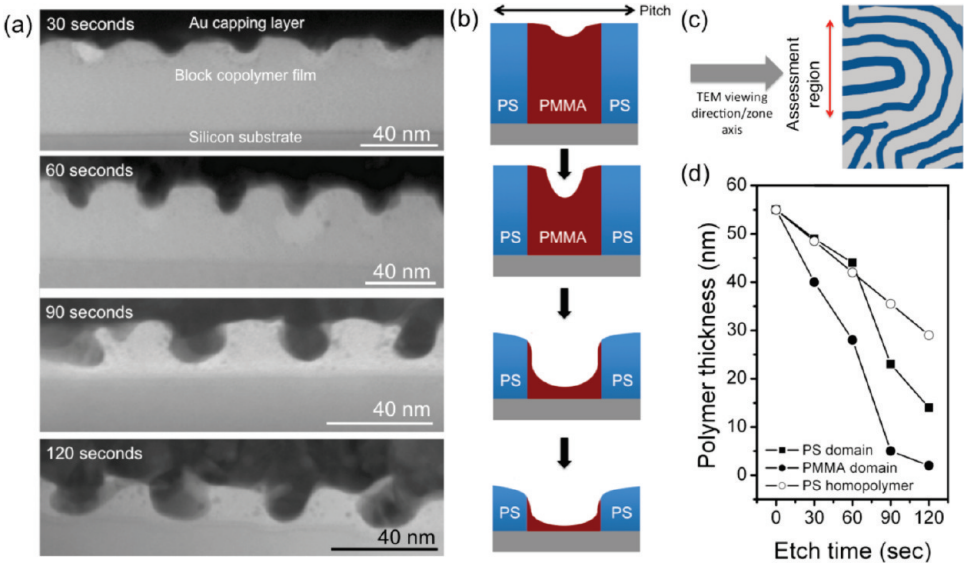

Figure 3. (a) Progressive PMMA removal *ex situ* TEM images of films after various etch periods (conditions 40 sccm CHF_3/5 sccm O_2 at 10 mTorr and 10 °C). (b) Schematic representing the PMMA removal process. (c) Schematic to show only PS lines (red arrow) which are near-parallel to the viewing axis/zone axis direction are analyzed. (d) Plot of PS domain and PMMA domain thickness as determined by cross-sectional TEM as a function of RIE time. The PS homopolymer thickness is also plotted for comparative purposes.

(under- vs over-etch), the most critical parameter. Figure 1a−d is a topographic AFM study of various etch times for the PMMA removal step. The PS-*b*-PMMA film was annealed for 120 h on a neutral PS-*r*-PMMA brush layer and was deposited from a 1.5 wt % solution. The film adopts a characteristic vertical oriented structure with natural periodicity of 42 nm based on FFT analysis. Although the AFM can be used to determine that the fingerprint pattern remains intact throughout the entire process and that PMMA removal is taking place (increase in *z*-height from 6 to 30 nm over 120 s etch), the *z*-height serves only as a qualitative guide for PMMA removal due to tip convolution effects. The film has an overall thickness of ∼56 nm (inclusive of polymer brush) as determined by TEM. The line widths for the PS and PMMA are ∼21 nm each as previously determined by other reports for the given molecular weight.[23] Figure 2, a 70° tilt cross SEM image, displays the structure of a PS-*b*-PMMA film after 120 s exposure to RIE. On the basis of SEM images, it was not possible to ascertain whether a residual layer existed or if the critical dimension (CD)/etch anisotropy of the final structures was altered due to SEM resolution limits and charging effects.

To gain a better insight into the PMMA removal step, cross-sectional TEM was employed to resolve the end point of the etch, monitor PMMA loss, and measure the PS line width loss where possible. Briefly, samples were coated with a 25 nm gold layer by electron beam evaporation after etching to enhance the mass−thickness contrast as carbon has a low atomic number and to provide additional protection of the film and profile during the TEM preparation.[24] The analysis was performed at bright field conditions (BF) with minimum exposure in order to minimize any possible beam damage affects. Because of the superior conformity of the coating, only silicon and silicon dioxide are generally visible in this TEM mode, but by creating contrast, it was possible to identify the etch pits and PS profile formed during etching. Non site-selective TEM sample preparation, using a series of grinding and precision argon polishing steps, was employed to prepare an electron transparent sample (refer to Supporting Information section 1). Figure 3a represents the TEM cross section at various time intervals throughout the PMMA removal process. TEM cross-sectional inspection of random arrays must be treated with caution as sectioning is not site-selective so adequate time and care must be given to ensure that the arrays of interest are aligned parallel to the zone axis/incident beam (Figure 3c). At 30 s, the removal of PMMA can be detected by the emergence of etch pits within the center of the PMMA domains. At 60 s, the etch has stabilized and the etch pits are clearly visible. Since we employ an RIE process where both physical and chemical processes are occurring, we must concede that the etch will cause some faceting of the structures (rounding of the PS line)—this becomes apparent at the 60 s interval although it is not excessive. Figure 3d is a plot of etch time as a function of the PS block, the PMMA block, and the PS homopolymer thickness. Progressive etching for 120 s shows that the majority of the PMMA has been removed. A residual rounded PMMA layer with a thickness of 1−3 nm remains which may also be the remnants of polymer brush (Figure 3b). The TEM used for this analysis could not resolve the interface between the residual polymer and the silicon. The final PS thickness was 14 nm, which indicates that the etch rates for homopolymers and diblock copolymers are different. This value differs substantially to the value of 31 nm recorded by AFM for the 120 s etch depth (Figure 1D). The AFM value may be improved upon by using ultrasharp AFM tips. Such deviation in etch rates may originate from the difference in molecular weight, film thickness, or glass transition temperature (T_g) of the homopolymer films.[25] Furthermore, the unique geometry of the lamellar structure and the fact that all RIE processes have some isotropic behavior may also impose a change in etch rates for both PS and PMMA in the

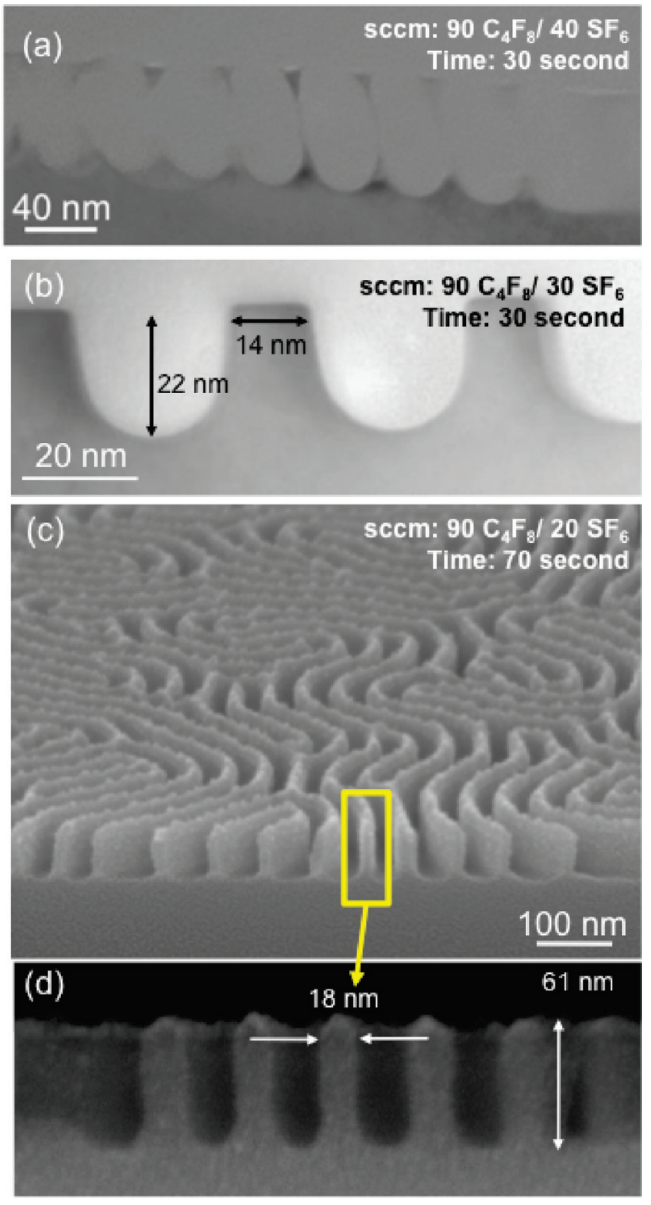

Figure 4. Silicon etching of the polystyrene lines with various SF_6 flow rates: (a) cross-sectional TEM after 30 s etch with 90 sccm C_4F_8/40 sccm SF_6 etch; (b) cross-sectional TEM after 30 s etch with 90 sccm C_4F_8/30 sccm SF_6 etch; (c) 70° tilt SEM image; and (d) 90° tilt SEM image in backscattered detector mode after 70 s etch with 90 sccm C_4F_8/20 sccm SF_6 etch. Note: the PMMA removal was 120 s.

diblock copolymer. Although the PMMA removal is successful with an overall etch rate of ∼27 nm/min (PMMA homopolymer etch rate of 45 nm/min), PS removal with an etch rate of ∼21 nm/min (PS homopolymer etch rate of 13 nm/min) provides an etch selectivity close to 1.3. Determining accurate PS line width becomes difficult as the etch progresses because the PS lines are not aligned precisely with the zone axis and polymer stability is perturbed at high etch times. The PMMA removal originates from the center of the PMMA domain and undergoes isotropic etching over the 120 s. The PS thickness is reduced because of the physical nature of the etch, but lateral etching is negligible during the PMMA removal step. Although it is not possible to determine the PS line width or lateral etching precisely, it can be concluded that PS line width loss is negligible and could easily be determined if the nanopatterns were aligned.

To complete the pattern transfer study, Figure 4 displays SEM and TEM images of a PS pattern (where the PMMA was

removed by etching for 120 s) transferred to the underlying bulk silicon substrate. Subtle changes in gas flow rates during ICP etching can have profound effects on the isotropic etch behavior of the silicon etch at these dimensions. To highlight the need for precision etching, we present three silicon etches whereby the SF_6 flow rates differ by only 20 sccm. Figure 4a displays a TEM image from a 30 s etch with flow rates of 90 sccm C_4F_8 and 40 sccm SF_6. Under these conditions the etch is extremely anisotropic and undercutting is particularly severe. The silicon lines are 3 nm in thickness and are susceptible to line collapse. Reducing the flow rate of the SF_6 to 30 sccm curtails this anisotropic behavior. The lower SF_6 flow rate of 30 sccm highlights that the transfer was partially successful, but the residual rounding of the PMMA structure at the base (from 120 s etch) has been translated into the substrate (curved profile at base). The replicated line pattern in the silicon has a line width of 14 nm and represents a loss of 7 nm (3.5 nm lateral etch rate) over a 30 s etch interval. The etch depth was calculated to be 22 nm (etch rate of 44 nm/min), whereas the predetermined etch rate was 60 nm for a 1 min etch. Again, further reduction in the flow rate to 20 sccm resulted in a highly anisotropic etch, which in turn allowed for the fabrication of high aspect ratio lines in the silicon (Figure 4c,d). A line width of 18 nm and a final etch depth of 60 nm (etch rate of 51 nm/min) were achieved. The increase in C_4F_8 to SF_6 ratio provides additional side-wall passivation (formation of CF_2), allowing for the fabrication of vertical profile silicon nanostructures. A similar trend has been reported for silicon nanolines (although an order of magnitude greater in dimension) whereby a ratio of 5:2 C_4F_8:SF_6 resulted in anisotropic etching and ratios close to 1:1 C_4F_8:SF_6 lead to isotropic etching and destruction of the patterns.[26] Prolonged etching beyond 60 nm was limited by the 15 nm polystyrene film as the PS line is extremely thin after 60 s of silicon etching. Overall, aspect ratios of 3:1 (61 nm deep and 18 nm wide) could be created in the underlying silicon substrate with a negligible loss in critical dimension (~3 nm) by employing TEM techniques to first establish the end point of the PMMA removal step. It is important for the PMMA removal step to be effective as any residual PMMA can limit the fidelity of the pattern transfer (Supporting Information S2). Metal contrast layers can also be employed to evaluate the PS residual layer post silicon etching (Supporting Information S3).

Conclusion

The *ex situ* TEM/metal contrast layers approach can provide abundant data on etch rate, over etch/end point detection, and film thickness, but its ability to determine CD loss is limited during the final etch moments as the structures tend to collapse and become difficult to image. We believe this could be circumvented by using aligned (physical or chemical) rather than random block copolymer patterns. The *ex situ* TEM technique requires that prior knowledge of the orientation, wetting layers, and 3D structure of the film is known to avail of this method as the RIE etchs both blocks. Our current study also reveals that homopolymer etch rates are good indicators for identifying etch conditions, but they do differ considerably from diblock etching. The fidelity of the pattern transfer to the underlying silicon is dependent on the initial PS profile and the anisotropic behavior of the silicon etch, but high aspect ratio structures can be achieved with careful control of etch parameters. The metal contrast layer approach could potentially be extended to other block copolymer patterns provided some prior knowledge of the film substructure is known. Finally, utilizing well-aligned block copolymer patterns[27,28] of known directionality will provide more consistent data for extracting line widths when compared to nonaligned patterns.

Acknowledgment. The authors acknowledge the following Science Foundation Ireland (SFI) grants for funding which supported this work: Grant 03-IN3-I375, CRANN CSET Grant, and the National Access Program at the Tyndall National Institute (Project No. 132). Dr. Nikolay Petkov acknowledges SFI Financial Grant 09-SIRG-I1621 for additional microscopy analysis. The authors are grateful to Intel Ireland for access to microscopy facilities and Prof. P. F. Nealey (University of Wisconsin) for providing some of the samples used for this study.

Supporting Information Available: Further information on the detailed TEM sample preparation, pattern transfer to silicon post incomplete PMMA removal, and PS residual layer analysis. This material is available free of charge via the Internet at http://pubs.acs.org.

References and Notes

(1) Bita, I.; Yang, J. K. W.; Jung, Y. S.; Ross, C. A.; Thomas, E. L.; Berggren, K. K. *Science* **2008**, *321*, 939.
(2) Ruiz, R.; Kang, H. M.; Detcheverry, F. A.; Dobisz, E.; Kercher, D. S.; Albrecht, T. R.; de Pablo, J. J.; Nealey, P. F. *Science* **2008**, *321*, 936.
(3) Stoykovich, M. P.; Kang, H.; Daoulas, K. C.; Liu, G.; Liu, C. C.; de Pablo, J. J.; Mueller, M.; Nealey, P. F. *ACS Nano* **2007**, *1*, 168.
(4) Darling, S. B. *Prog. Polym. Sci.* **2007**, *32*, 1152.
(5) Asakawa, K.; Hiraoka, T. *Jpn. J. Appl. Phys., Part 1* **2002**, *41*, 6112.
(6) Liu, C. C.; Nealey, P. F.; Ting, Y. H.; Wendt, A. E. *J. Vac. Sci. Technol. B* **2007**, *25*, 1963.
(7) Ting, Y. H.; Park, S. M.; Liu, C. C.; Liu, X. S.; Himpsel, F. J.; Nealey, P. F.; Wendt, A. E. *J. Vac. Sci. Technol. B* **2008**, *26*, 1684.
(8) Zhang, M. F.; Yang, L.; Yurt, S.; Misner, M. J.; Chen, J. T.; Coughlin, E. B.; Venkataraman, D.; Russell, T. P. *Adv. Mater.* **2007**, *19*, 1571.
(9) Zschech, D.; Kim, D. H.; Milenin, A. P.; Scholz, R.; Hillebrand, R.; Hawker, C. J.; Russell, T. P.; Steinhart, M.; Gosele, U. *Nano Lett.* **2007**, *7*, 1516.
(10) Thurn-Albrecht, T.; Steiner, R.; DeRouchey, J.; Stafford, C. M.; Huang, E.; Bal, M.; Tuominen, M.; Hawker, C. J.; Russell, T. P. *Adv. Mater.* **2000**, *12*, 787.
(11) Ramanathan, R.; Nettleton, M.; Darling, S. B. *Thin Solid Films* **2009**, *517*, 4474.
(12) Ito, T.; Okazaki, S. *Nature* **2000**, *406*, 1027.
(13) Wallraff, G. M.; Hinsberg, W. D. *Chem. Rev.* **1999**, *99*, 1801.
(14) Cheng, J. Y.; Mayes, A. M.; Ross, C. A. *Nature Mater.* **2004**, *3*, 823.
(15) Li, W.; Sheller, N.; Foster, M. D.; Balaishis, D.; Manners, I.; Annís, B.; Lin, J.-S. *Polymer* **2000**, *41*, 719.
(16) Jung, Y. S.; Ross, C. A. *Nano Lett.* **2007**, *7*, 2046.
(17) Cheng, J. Y.; Pitera, J.; Park, O. H.; Flickner, M.; Ruiz, R.; Black, C. T.; Kim, H. C. *Appl. Phys. Lett.* **2007**, *91*, 143160.
(18) Han, E.; Stuen, K. O.; Leolukman, M.; Liu, C. C.; Nealey, P. F.; Gopalan, P. *Macromolecules* **2009**, *42*, 4896.
(19) Park, S. M.; Yun, S. H.; Sohn, B. H. *Macromol. Chem. Phys.* **2002**, *203*, 2069.
(20) Tang, C. B.; Lennon, E. M.; Fredrickson, G. H.; Kramer, E. J.; Hawker, C. J. *Science* **2008**, *322*, 429.
(21) Zschech, D.; Milenin, A. P.; Scholz, R.; Hillebrand, R.; Sun, Y.; Uhlmann, P.; Stamm, M.; Steinhart, M.; Goesele, U. *Macromolecules* **2007**, *40*, 7752.
(22) Zhang, C. C.; Yang, C. S.; Ding, D. F. *Appl. Surf. Sci.* **2004**, *227*, 139.
(23) Liu, G.; Stoykovich, M. P.; Ji, S.; Stuen, K. O.; Craig, G. S. W.; Nealey, P. F. *Macromolecules* **2009**, *42*, 3063.
(24) Fitzgerald, T. G.; Farrell, R. A.; Petkov, N.; Bolger, C. T.; Shaw, M. T.; Charpin, J. P. F.; Gleeson, J. P.; Holmes, J. D.; Morris, M. A. *Langmuir* **2009**, *25*, 13551.
(25) Vourdas, N.; Boudouvis, A. G.; Gogolides, E. *J. Phys.: Conf. Ser.* **2005**, *10*, 405.
(26) Wang, X.; Chen, Y.; Wang, L.; Cui, Z. *Microelectron. Eng.* **2008**, *85*, 1015.
(27) Kim, S. O.; Solak, H.; Stoykovich, M. P.; Ferrier, N. J.; de Pablo, J. J.; P.F., N. *Nature* **2003**, *424*, 411.
(28) Park, S.-M.; Stoykovich, M. P.; Ruiz, R.; Zhang, Y.; Black, C. T.; Nealey, P. F. *Adv. Mater.* **2007**, *19*, 607.